# URBEX: A VALIDATED, FAST-RUNNING CODE TO COMPUTE BLAST EFFECTS IN URBAN CONFIGURATIONS

MAROUA HEDHLI[1], EMMANUEL LAPÉBIE[1], ERNHOLLA MARINASY[1] & ISABELLE SOCHET[2]
[1]Apex Solutions, France
[2]PRISME Laboratory, France

ABSTRACT

This paper presents the URBEX fast-running code, one of the outputs of the research project URB(EX)$^3$, co-funded by the French National Research Agency (grant #ANR-21-CE39-0016). The URBEX code is able to compute all urban effects following an explosion in urban configurations (multiple diffractions, regular and Mach reflections, channelling and urban canopy bypassing) in less than 2 minutes on a standard laptop, without the need of specific modelling knowledge so it could be used by first responders in emergency situations. Urban configurations are retrieved from widely available geographic data (OpenStreetMap, the IGN Institute in France or other sources). The URBEX code relies on a breakthrough approach, far above the international state-of-the-art, and its underlying mathematical method has been patented. This method will be detailed and discussed in the paper, together with its current limitations and the planned future improvements. A number of comparisons with high-quality, small-scale experiments done in the PRISME laboratory will also be presented, as well as with results from numerical codes and forensic analysis of past bombings. Finally, current actions aimed to extend the URBEX method will be outlined, in particular the development of fast-running codes for explosions in complex buildings and in tunnel networks (MALBEC project, cofounded by the French Innovation Defense Lab).

*Keywords: fast-running code, explosion, blast effects, urban configurations.*

## 1 INTRODUCTION

Explosion risks, whether accidental or intentional, pose a major threat to people and property in various environments, including industrial, public, and military areas. Past disasters like those in Seveso (Italy) 1976, Toulouse (France) 2001, and Beirut (Lebanon) 2020 highlight the severe consequences. Understanding explosion dynamics is essential for developing a rigorous fast-running model to simulate explosions, particularly in urban and confined spaces, where shock wave reflections and diffractions add complexity to the analysis.

Currently, only costly three-dimensional computational fluid dynamics (CFD) methods can accurately predict blast loads. Tools like BlastFoam [1] and Viper::Blast [2] have shown potential in modelling complex blast scenarios. Unfortunately, these techniques are not suitable for certain applications where a short execution time is required. Based on the authors' knowledge, limited efforts have been made to develop fast-running models. One promising approach involves the use of neural networks [3], [4]. This method requires a significant amount of reliable data to train the network, and its ability to generalize to other configurations has yet to be fully established. Another, more relevant method is the use of composite approaches. In fact, tools like 3D Blast from ARA (Applied Research Associates) [5], provide simplified solutions for blast load calculations on isolated buildings. Fi-Blast [6], [7] and VAPO [8] offer more comprehensive approaches, although no real configuration data has been published. In France, the FLASH code [9]–[12], developed at CEA/DAM, is the most advanced, using a shortest path method, diffraction model, and discretized volume approach for channelling. The URB(EX)$^3$ research project, including a detailed review of

 
www.witpress.com, ISSN 1743-3509 (on-line)
doi:10.2495/SUSI250051

existing approaches, URBEX code requirements, and comparison of results, was presented in Chereau et al. [13].

This study aims to develop an innovative, fast-running, meshless model for evaluating blast consequences in urban environments. The proposed modelling approach utilizes advanced computational methods to simulate blast effects efficiently. The performance of the new model is compared with experimental data, numerical simulations, and real-world event data to assess its accuracy and reliability.

## 2 PRINCIPLE OF ANALYTICAL CODE

### 2.1 A new approach to presenting the problem

The URBEX model is based on a spatial vision of the propagation of the air shock wave (Fig. 1(a)), rather than temporal evolution as in numerical approaches (Fig. 1(b)). It describes the spatial domains of a succession of unit waves generated by various physical phenomena (diffractions, regular and Mach reflections, channelling and urban canopy bypassing), all resulting from the initial wave emitted at the explosion point. The characteristics of each unit wave in its spatial domain are known analytically based on a functional approach, no meshing being required. The model developed is very innovative and has never been described in the literature (the patent [14] has already been filed).

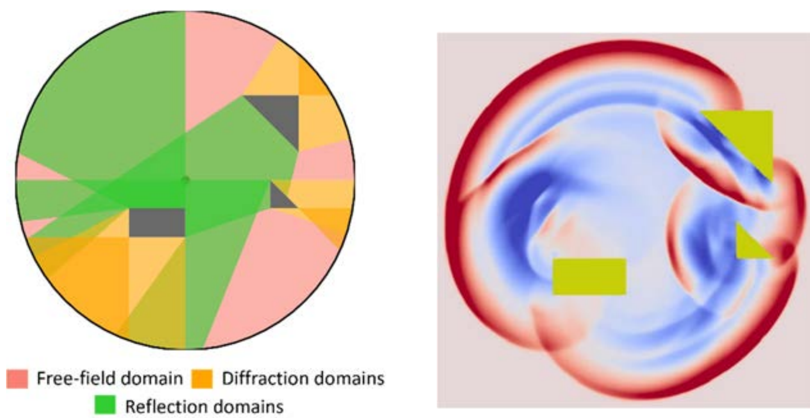


(a) (b)

Figure 1: Comparison of spatial vs temporal evolution of a wave. (a) Spatial domains of the URBEX Model, Level 1; and (b) Temporal evolution of a wave Viper::Blast.

The model describes a tree of unitary waves, where level 0 corresponds to the initial 'free-field' wave, and level $i + 1$ includes the unitary waves resulting from the reflections and diffractions of the waves from generation $i$. Each wave of level $i$ can be treated as a new initial wave, which in turn generates diffracted and reflected waves of level $i + 1$, and so on. This recursive approach is depicted in Fig. 2. Each unitary wave of level $i$ is described by:

- The reference to its parent wave of level $i - 1$.
- An influence zone (visibility polygon, apex, angular range, supporting segment).
- An analytical function that provides the various parameters of the Friedlander function.

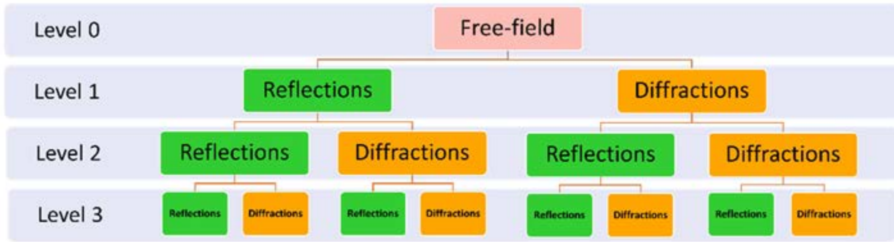


Figure 2: Recursive tree structure of unitary waves.

For each point of interest, all relevant zones it belongs to are identified. Then, the contribution of each wave is calculated by tracing back through the recursion tree to the direct wave.

Using a simple example with a charge and three obstacles, Fig. 1 shows the visibility polygon of the free-field wave in pink. This is level 0 in the tree structure. From this parent wave, we have six diffractions, represented by six diffraction visibility polygons in orange, and three reflections, represented by three reflection visibility polygons. These diffractions and reflections represent level 1 in the tree structure.

### 2.2 Unit waves superposition

It is assumed that at each point in the domain, the received pressure signal is the sum of unit signals. Fig. 3 demonstrates a simple example of unit wave superposition. The free-field wave (blue path) of level 0 produces a reflection (orange path) and a diffraction (green path) wave of level 1 at the point of interest. The final signal at this point consists of three peaks: the first corresponds to the free-field wave, the second to the reflected wave, and the third to the diffracted wave. The strength of our new approach lies in calculating $N$ waves instead of just calculating the wave that passes through the shortest path [9]–[12].

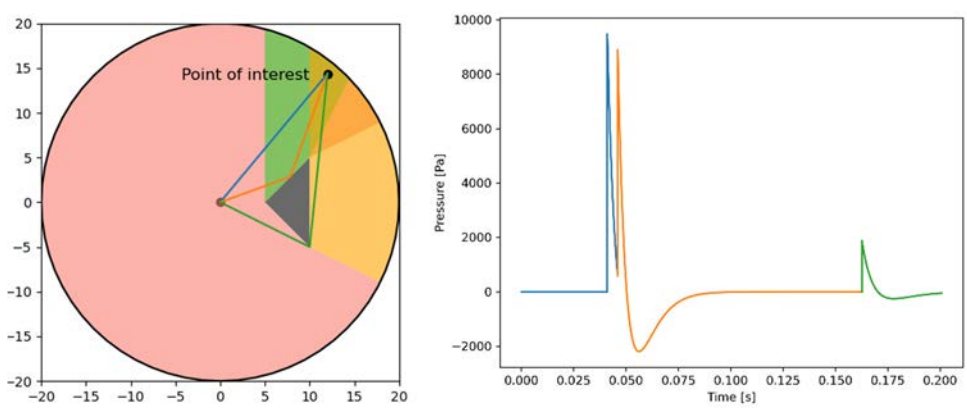


(a) (b)

Figure 3: Principle of unit waves superposition. (a) Simple case, different paths to reach the point of interest. Level 1; and (b) Sum of unit signals calculated for each path.

### 2.3 URBEX model: Free-field processing

In this study, new fits are developed as several limitations in the previous approaches are identified [15]. The old fits were often redundant, sometimes inconsistent, and lacked physical coherence. Furthermore, they required numerous coefficients, which led to frequent errors, and some were non-invertible, making the calculation of the reduced distance more complex. It may be recalled that the reduced distance is defined as follows:

$$Z = \frac{R}{\sqrt[3]{m}}, \tag{1}$$

where $m$ is the explosive hemispherical mass and $R$ is the true distance in metres.

To solve these issues, a new approach was adopted. Redundancies were eliminated and a lower bound for reduced distance was set. Additionally, reversible fits were chosen, allowing for a more accurate and consistent calculation of the reduced distance.

#### 2.3.1 Lower bound for reduced distance

$Z$ can be related to the non-dimensional radius ratio $\frac{R}{R_0}$, $R_0$ being the spherical charge radius, as follows:

$$Z = \frac{R}{\sqrt[3]{m}} = \frac{R}{\sqrt[3]{\frac{4}{3}\pi {R_0}^3.\rho_0}} = \frac{1}{\sqrt[3]{\frac{4}{3}\pi.\rho_0}} \frac{R}{R_0}, \tag{2}$$

where $\rho_0$ is the high explosive density.

It should be noted that the fireball radius $R_{\text{fireball}}$ is 25 to 35 times the charge radius $R_0$ for most solid high-explosives. A commonly agreed value for TNT is $30.R_0$, which corresponds to $Z \sim 1.6$. Inside the fireball, phenomena strongly differ from free-field shock propagation, and we consider that it is useless to try modelling waveform evolution below this threshold.

Moreover, $Z = 3$ (for TNT) is considered to be the upper threshold for which blast consequences are extremely severe, both for humans and structures. It is thus not important to be precise below $Z = 3$ since everything will be destroyed/everybody will be killed.

#### 2.3.2 URBEX free-field fits for TNT

We aim to obtain the evolution of the different parameters of the Friedlander as a function of the reduced distance for each unit wave. Indeed, regardless of the phenomenon being studied (diffraction or reflection), it is reduced to a free-field equivalence. We will then recalculate the reduced distance differently using the appropriate function and then use our free-field fits to find the different parameters.

Instead of providing a model for the maximum overpressure $\Delta P_+$, the equivalent option of modelling the shock Mach number $M$ (wave speed divided by sound speed) was chosen instead. Both variables are related through:

$$\frac{\Delta P_+}{P_0} = \frac{2\gamma}{\gamma+1} \ (M^2 - 1), \tag{3}$$

with $\gamma$ the polytropic coefficient (ratio of specific heats) and $P_0$ the atmospheric pressure.

The mathematical expression proposed for reduced Mach variation is:

$$M^2(Z) = \left(a_0 + a_1 \frac{Z}{Z_0} + a_2 \left(\frac{Z}{Z_0}\right)^2\right)^{-\frac{1}{n}} + 1, \tag{4}$$

with $Z_0 = 1 \frac{\mathrm{m}}{\sqrt[3]{\mathrm{kg}}}$ to have non-dimensional coefficients.

Since overpressure and Mach number are related, knowing the evolution of Mach with $Z$, the expression for the reduced overpressure can then be derived; this is given by the following formula:

$$\Delta P_+(Z) = P_0 \times \frac{2\gamma}{\gamma+1} \times (M^2(Z) - 1). \tag{5}$$

The expression of the reduced time of arrival is as follows:

$$\overline{t_a}\,(Z) = \overline{t_{a,\mathrm{ref}}}\,(Z_{\mathrm{ref}}) + \int_{Z_{\mathrm{ref}}}^{Z} \frac{dZ}{a_0 . M(Z)}, \tag{6}$$

in which $M$ is the shock Mach number, $a_0$ is the speed of sound and $\overline{t_{a,ref}}$ is the time of arrival at the reference reduced distance $Z_{\mathrm{ref}}$.

A fit for the reduced positive phase duration $\overline{\Delta t_+}$ is also needed; the following was chosen:

$$\overline{\Delta t_+} = b_0 + b_k \left(\frac{Z - Z_{\min}}{Z_0}\right)^k. \tag{7}$$

The impulse $\mathrm{I}_+$ can be computed from overpressure $\Delta P_+$, positive phase duration $\Delta t_+$ and exponential factor $\alpha$. The corresponding equation is:

$$\mathrm{I}_+ = \frac{\Delta P_+ \Delta t_+}{\alpha^2} (e^{-\alpha} + \alpha - 1). \tag{8}$$

### 2.4 Functional approach

The core reasoning of the URBEX model is based on determining the visibility polygons for each unit wave and on the fact that within each visibility polygon, pressure and impulse can be calculated analytically, with no meshing required. Each unit wave is associated with a function that computes, across the entire spatial domain, the different Friedlander parameters as a function of the reduced distance.

#### 2.4.1 Regular reflections

The initial wave (level 0) propagates directly to every point in the study area that is visible from the initial explosion point. The corresponding signal is described at any point in this zone by the free-field functions presented previously. Each reflective surface generates a reflective unit wave. This unit wave seems to be emitted from a virtual source, see Fig. 4, symmetrical to the initial point in relation to the segment. It propagates within an angular sector defined by the segment. The corresponding signal, at any point in this area, is described by the free field functions $\Delta P_+(Z)$ derived from the virtual source.

As shown in Fig. 4(b), at the point of interest, the signal exhibits two main peaks: one peak corresponds to the wave arriving directly, and the other to the wave that will reflect and come from a virtual source. The second peak arrives slightly later, as it travels a longer path.

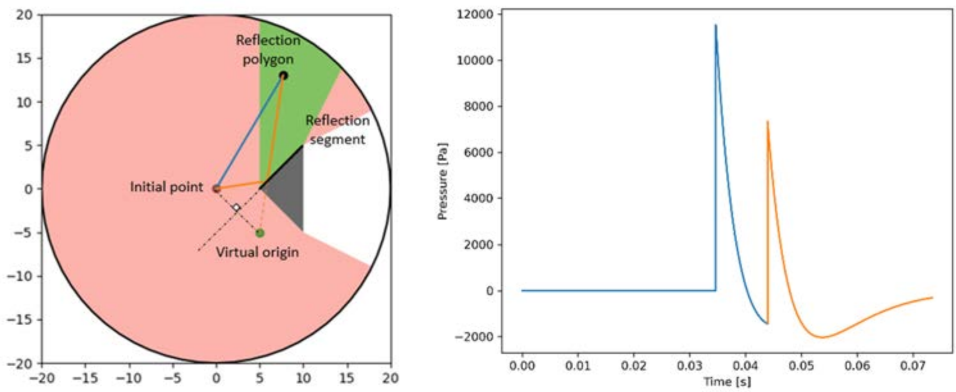


(a) (b)

Figure 4: Principle of the mirror-image approach. (a) Path of the direct wave (in blue) and path of the reflected wave (in orange); and (b) Signal with two main peaks.

The mirror-image approach for handling regular reflections is strictly valid for sound waves. In the case of intense shock waves, it is important to quantify the error introduced by the sonic approximation, especially with regard to the reflection coefficient at the reflective surface, which is currently set to 2.0. A correction factor must be applied to the overpressure in the region affected by the regular reflected wave (excluding the Mach domain). In this paper, we only present the simple version of URBEX, which does not include the new model of regular reflection.

2.4.2 Diffractions approach

As shown in Fig. 5, each corner of a building meeting certain criteria generates a diffracted wave. This wave propagates from the diffraction apex $A$, in an angular sector (diffraction polygon) limited by a building surface (reference segment) and a segment of the free-field zone which we call line of sight. The corresponding signal is described at every point of this diffraction polygon by the Bazhenova et al. [16] functions at the apex and by the free-field decay when moving away from the apex.

The approaches of Whitham [17], [18] (theoretical relationship between the section of a shock tube and the Mach number) and Bazhenova et al. [16] (empirical, based on the

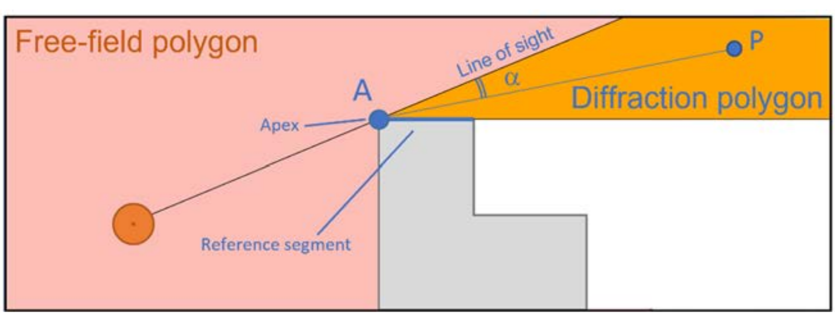


Figure 5: Simple diffraction model.

experimental results of skews [19], [20]) relate the Mach number after diffraction to the Mach number before diffraction and the diffraction angle. This approach is similar to the concept of a 'singular pressure drop' in incompressible fluid mechanics. As shown in Fig. 6, the diffraction point (apex) causes a sudden drop in pressure (or Mach number), except in the region near the apex, where the behaviour becomes more complex. This phenomenon can also be modelled by an instantaneous increase in the reduced distance $Z$, referencing the free-field curves.

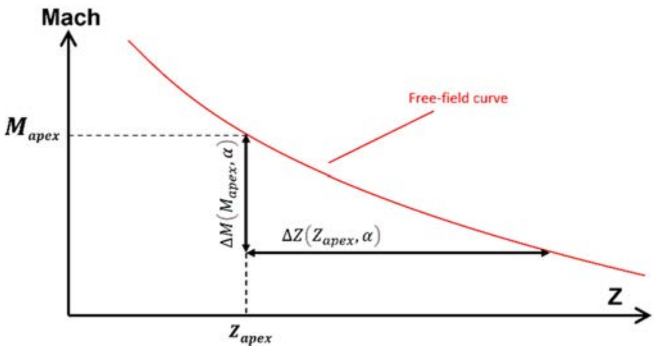


Figure 6: Diffraction apex influence on the evolution of the Mach number, with reference to the free-field curve.

The Bazhenova model consists in determining the reduced distance $Z$ of any point $P$ within the diffraction polygon, at a distance $AP$ from the apex, and observed at an angle $\alpha$ relative to the line of sight, by summing:

- The reduced distance at the apex $Z_{\text{apex}}$.
- A sudden increase $\Delta Z(Z_{\text{apex}}, \alpha)$ resulting from the decrease $\Delta M(M_{\text{apex}}, \alpha)$ in the Mach number between the incident Mach number $M_{\text{apex},0}$ and the Mach number calculated for the $\alpha$ angle, $M_{\text{apex},\alpha}$.
- The reduced distance corresponding to the account of the distance $AP$, $\Delta Z_{AP}$.

The evolution of the Mach number at the apex according to Bazhenova is given by the following formula:

$$M_{\text{apex},\alpha} = 1 + \left(M_{\text{apex},0} - 1\right)\left(1 - \sin\left(\frac{\alpha}{2}\right)\right), \tag{9}$$

from which we can simply derive:

$$\Delta M\left(M_{\text{apex}}, \alpha\right) = -\left(M_{\text{apex},0} - 1\right)\sin\left(\frac{\alpha}{2}\right). \tag{10}$$

For a point $P$ in the diffraction polygon at a distance $\Delta Z_{AP}$ from the apex, the reduced distance is expressed as:

$$Z = Z_{\text{apex}} + \Delta Z\left(Z_{\text{apex}}, \alpha\right) + \Delta Z_{AP}. \tag{11}$$

The diffraction approach employed in the basic URBEX model is relatively conservative, as it results in an overestimation of the Mach number after diffraction due to the expansion zone defined by the angle beta. Specifically, the Bazhenova model tends to overestimate the overpressure when the point of interest lies within the expansion zone, assuming that the overpressure remains equivalent to that in the free-field, since the point falls within the visibility polygon of level 0. This paper presents the basic version of URBEX, excluding the newly developed diffraction model that incorporates the angle beta and the initiation of diffraction within the expansion zone.

## 2.5 Other urban effects

### 2.5.1 Mach reflection

When a wave of level $i - 1$ generates, from the same reflecting segment, both a regular wave and a Mach wave, a Boolean operation on the representative polygons of these waves can be used to avoid double-counting the reflected wave. The positioning of the contact point will determine the function to prioritize in order to calculate the different parameters of the unit wave. Fig. 7 shows the overlap of regular reflection areas with Mach reflection areas. This paper presents only the basic version of URBEX, which excludes Mach reflection.

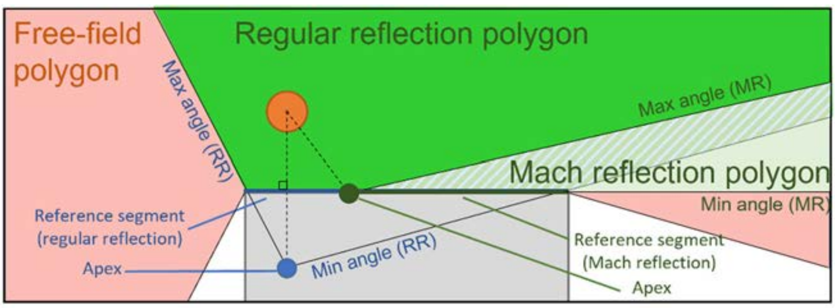


Figure 7: Overlap of regular reflection areas and Mach reflection areas.

### 2.5.2 Channelling

Urban canyon effects lead to a gradual transition from a 3D free-field wave to a 2D wave. The wave initially propagates spherically down the street, with reflections off the walls that result in Mach reflections. At a certain distance from the source, the propagation evolves into a cylindrical shape, concentrating the energy along the street and increasing the wave's intensity. This results in a reduced pressure drop compared to free-field conditions, potentially leading to larger danger zones.

### 2.5.3 Urban canopy bypassing

What is currently being calculated is the behaviour on the ground, but another possibility is that the wave could bypass the building from above. This wave will be highly diffracted, so the expected overpressures are not very high. This allows for overpressures to be mapped in the case of a building with an inner courtyard. The wave inside arrives with low intensity and is significantly delayed compared to the other waves. This paper discusses only the basic version of URBEX, omitting the urban canopy wave.

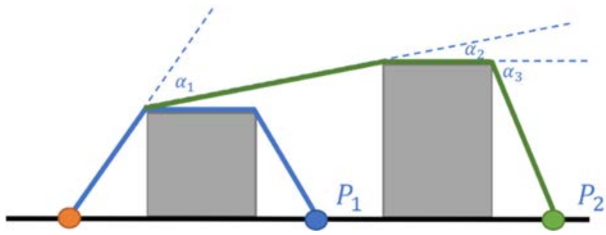


Figure 8: Example of an 'urban canopy' wave.

## 3 URBEX APPLICATIONS AND RESULTS

The URBEX model can calculate a complex wave at every point in the area of interest, taking into account all urban effects: regular and Mach reflections, diffractions, shock wave channelling, and bypassing by the urban canopy. In this section, we will present the results obtained with the basic version of the model, which does not include the improved diffraction model, the new regular reflection model, Mach reflections, or the urban canopy wave.

### 3.1 Comparison for urban configurations

A first comparison is conducted with the DEMOCRITE platform (image courtesy of IT Link), which uses the CEA/DAM FLASH code [9]–[12]. The scenario involves the explosion of a 'small vehicle' (227 kg TNT, following FEMA standards [21]) in a large square in the city of Cahors (France). Fig. 9 compares the FLASH results with the numerical simulation results from the Viper::Blast software and an URBEX simulation at precision level 1. The node spacing (FLASH) is 2 m, while the pixel size (URBEX) is $300^2$. The output displays danger zones based on overpressure thresholds in accordance with French regulations, where Zone 1 (red) is 0.430 mbar, Zone 2 (orange) is 0.2 mbar, Zone 3 (yellow) is 0.140 mbar, Zone 4 (green) is 0.050 mbar, and Zone 5 (blue) is 0.02 mbar. The coloured circles represent the corresponding free-field danger zones.

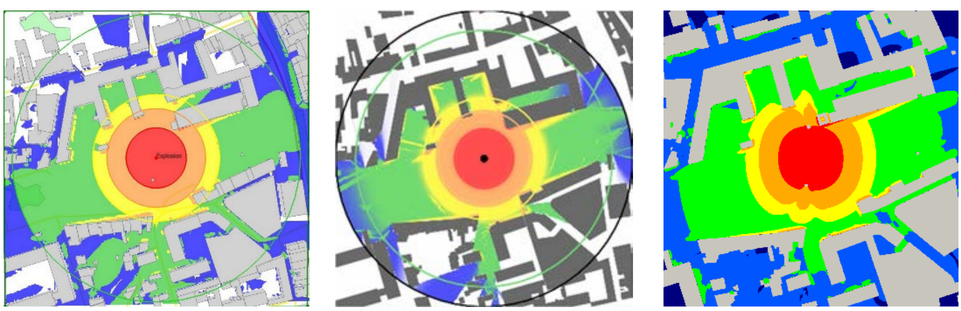

(a) (b) (c)

Figure 9: Danger zones calculated using (a) FLASH (courtesy of IT Link), runtime = 41 s; (b) URBEX: precision level 1, runtime =18 s; and (c) Viper::blast, runtime = 34 min.

At precision level 1, URBEX outperforms FLASH by delivering nearly identical results with almost half the execution time. It also shows performance comparable to the

Viper::Blast software, which requires 34 minutes for execution, although URBEX achieves similar results in a significantly shorter time. The free-field danger zones are comparable across all three methods.

A second comparison is made with Viper::Blast and the experimental results of INSA-CVL using a charge of propane/oxygen mixture at small scale. The event involves an explosion equivalent to a hemispherical charge of 1,777 kg TNT occurring in the Butte-aux-Cailles district of Paris (France). As illustrated in Fig. 10, the results obtained with URBEX at level 1 are similar to those found with the Viper::Blast simulation software as well as the experimental results, which proves that our model is reliable and accurate in simulating an explosion in an urban environment.

(a) (b) (c)

Figure 10: Danger zones calculated using (a) Viper::Blast; (b) experimental results of INSA-CVL; and (c) URBEX with precision level 1.

### 3.2 Application to the Oslo bombing

Christensen and Hjort [22] provide a forensic analysis of the Oslo bombing occurred on 22 July 2011, including field surveys to determine the percentage of broken windows on various façades near the explosion. Fig. 11 compares this analysis with URBEX results. It uses the Green Book consequence model for glass breakage [23], applied to the signal’s maximum peaks. Some buildings were manually added to the OSM data (with a few still missing), as they were demolished after the event. Glass breakage is strongly influenced by diffraction effects, making it highly non-isotropic. The red zone generated by URBEX, indicating over

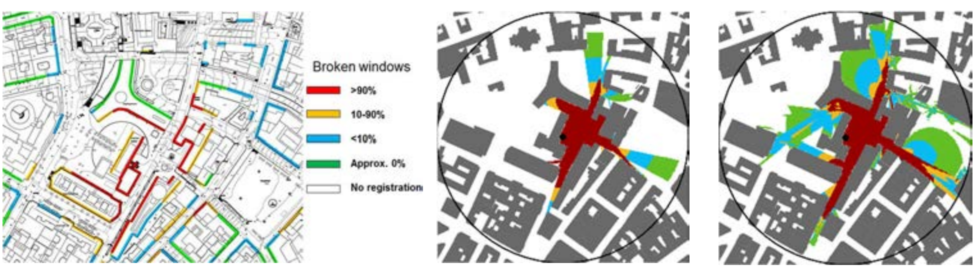


(a) (b) (c)

Figure 11: Percentage of broken windows from the Oslo bombing. (a) Ground truth [20]; URBEX results: (b) Precision level 1; and (c) Precision level 2.

90% of broken windows, closely matches the field data. Other areas provide more conservative estimates due to the simple Bazhenova diffraction model.

## 4 CONCLUSION AND FUTURE WORK

In this paper, we presented the basic model of URBEX and demonstrated its effectiveness through various results. These findings show that URBEX delivers reliable and accurate simulations, particularly in urban environments. The model proves to be efficient, with significant potential for future developments and applications. It is readily usable by first-responders in crisis situations (potential VB-IED for instance). Furthermore, URBEX's efficiency, especially at higher precision levels, highlights its value for applications requiring precise danger zone analysis. The URBEX code is set to define a new benchmark for fast and accurate computations of explosion consequences in urban environments. A separate paper will be devoted to presenting the new regular reflection model, the Mach reflection model, a more rigorous diffraction model, and urban canopy bypassing.

Extensions of this work are currently underway. The CONVEX project, co-funded by the MAIF foundation, is investigating the explosion risks associated with the thermal runaway of electric vehicle batteries in confined spaces such as underground car parks, tunnels, and ferries. The MALBEC project, co-funded by the French Defense Innovation Agency, is addressing the challenges of explosive breaching by Special Forces. It is developing a fast-running tool to assist in preparing such operations, which requires a 3D extension of the URBEX approach and modelling of quasi-static pressure generation and propagation.

## ACKNOWLEDGEMENTS

The authors would like to thank their partners, INSA-CVL and Blast Solutions & Associates, for their support and collaboration. They also wish to express their gratitude to the French National Research Agency for selecting and co-funding the URB(EX)$^3$ project. Furthermore, the authors appreciate the valuable discussions with the project's advisory board members: SAFE cluster, IRCGN, LCPP, CETID, PIAM, 17th RGP, IPE, IRSN, INERIS, EURENCO, BS&A, SPIEZ laboratory (CH), SSSL (UK), and other organisations that supported the project, including DGA, CEA/DAM, RisCrises, and CERL (CA).

## REFERENCES

[1] Synthetik Applied Technologies, BlastFoam: An OpenFOAM solver for compressible multi-fluid flow with application to high-explosive detonation, 2019.

[2] Stirling, C.G., Viper::Blast user manual. Stirling Simulation Services Limited: Glasgow, 2020.

[3] Dennis, A.A., Stirling, C. & Rigby, S.E., Towards the development of machine learning tools for blast load prediction. *Proceedings of the 6th International Conference on Protective Structures (ICPS6)*, International Association of Protective Structures, 2023.

[4] Dennis, A.A & Rigby, S.E., The direction-encoded neural network: A machine learning approach to rapidly predict blast loading in obstructed environments. *International Journal of Protective Structures*, 20414196231177364, 2023.

[5] 3D Blast, https://www.ara.com/3d-blast/. Accessed on: 24 Feb. 2025.

[6] Fi-Blast, Fast analysis of blast and fragment loaded structures. https://numerics.de/products/fi-blast/. Accessed on: 24 Feb. 2025.

[7] Tank, A., Greulich, B. & Rottenkolber, E., Rapid calculation of urban blast propagation using FI-BLAST. *Proceeding of 14th International Symposium on Interaction of the Effects of Munitions with Structures (ISIEMS14)*, Seattle, WA, USA, 2011.

[8] Nichols, J.F. & Doyle, G., Current engineering models and capabilities in the vulnerability assessment and protection option (VAPO) software. *Structures Congress*, 2014.

[9] Lapébie, E., Soulié, R. & Youinou, L., FLASH: Fast Lethality Assessment for Structures and Humans. *Proceeding of the 24th International Symposium on Military Aspects of Blast and Shock (MABS24)*, Halifax, Canada, 2016.

[10] Lapébie, E. et al., Fast-running models for blast and QSP in complex geometries. *Proceedings of the 17th International Symposium on Interaction of the Effects of Munitions with Structures (ISIEMS17)*, Bad-Neuenahr, Germany, 2018.

[11] Lapébie, E. et al., Fast-running models for blast and QSP in complex geometries. *Improved Explosives and Munitions Risk Management (IEMRM)*, MSIAC workshop, Granada, Spain, 2018.

[12] Osmont, A. & Lapébie, E., Models for rapid calculation of breath and quasi-static pressure in complex environments. *Proceeding in French Congress of Mechanics*, Brest, France, 26–30 Aug. 2019.

[13] Chereau, G., Lapébie, E. & Sochet, I., URBEX: A fast yet accurate model to compute blast consequences in urban geometries. *Proceeding of the 26th International Symposium on Military Aspects of Blast and Shock (MABS26)*, Wollongong, Australia, 2023.

[14] Lapébie, E. (inventor), *Procédé de gestion d'une explosion dans un environnement réel*. France Patent FR2400950. To be published.

[15] Swisdak, J.M., Simplified Kingery airblast calculations. *Proceedings of the 26th DoD Explosives Safety Seminar*, Aug. 1994.

[16] Bazhenova, V., Gvozdeva, L.G. & Nettleton, M.A., Unsteady interactions of shock waves. *Aerospace Sciences*, vol. 21, Pergamond Press, pp. 249–331, 1984.

[17] Whitham, G.B., A new approach to problems of shock dynamics: Part I Two dimensional problems. *Journal of Fluid Mechanics*, **2**(2), pp. 145–171, 1957.

[18] Whitham, G.B., *Linear and Nonlinear Waves*. John Wiley & Sons, 1974.

[19] Skews, B.W., The perturbed region behind a diffracting shock wave. *J. Fluid Mech.*, **29**, pp. 705–719.

[20] Skews, B.W., The shape of the diffracting shock wave. *J. Fluid Mech.*, **29**, pp. 297–304.

[21] Joint Counterterrorism Assessment Team (JCAT), Bomb threat standoff distances. https://www.dni.gov/nctc/jcat/references.html. Accessed on: 5 Mar. 2025.

[22] Christensen, S.O. & Hjort, O.J.S., Back calculation of the Oslo bombing on July 22nd, using windows breakage. *Proceeding of the 22nd International Symposium on Military Aspects of Blast and Shock (MABS22)*, Bourges, France, 2012.

[23] TNO, *Green Book – CPR 16E – Methods for the Determination of Possible Damage*, 1992.